Published paper:

B. Ban, S. Stipetić and M. Klanac, "Synchronous Reluctance Machines: Theory, Design and the Potential Use in Traction Applications," 2019 International Conference on Electrical Drives & Power Electronics (EDPE), 2019, pp. 177-188

http://dx.doi.org/10.1109/EDPE.2019.8883905

Synchronous Reluctance Machines: Theory, Design and the Potential Use in Traction Applications

Branko Ban
Dept. of El. Machines and Automation
FER; University of Zagreb;
Unska 3, 10000 Zagreb, Croatia
branko.ban@outlook.com

Stjepan Stipetić
Dept. of El. Machines and Automation
FER; University of Zagreb;
Unska 3, 10000 Zagreb, Croatia
stjepan.stipetic@fer.hr

Mario Klanac
Dept. of El. Machines and Automation
FER; University of Zagreb;
Unska 3, 10000 Zagreb, Croatia
mario.klanac@fer.hr

***Abstract*—The volatilities in the permanent magnet price have raised interest within the automotive industry for finding substitute electric machine designs. The proposed alternatives are synchronous reluctance machines (SyRM) and its derivatives, assisted synchronous reluctance (PMASR) machines. These solutions rely on high reluctance torque thus theoretically needing no magnet material in the rotor structure. This paper covers reluctance machine theoretical background, rotor parametrization, design alternatives, structural analysis, and optimization. Commercially available traction reluctance machines applications have been investigated. Marine and freight traction and commercial vehicle power take-off have been selected as application niches. Finally, a performance comparison for different saliency ratios of the ideal SyRM, ferrite and neodymium PMASR has been conducted.**

***Keywords*—electric machine; traction; permanent magnet; synchronous reluctance; assisted; optimization; comparison; axially laminated; design; power take-off; commercial vehicles; rare earth free.**

TABLE I. Abbreviation list

Abbreviation:	Desciption:
CFD	Computational fluid dynamics
DE	Differential evolution
FEM	Finite element method
FW	Field weakening
FOS	Factor of safety
IM	Induction machine
IPM	Interior permanent magnet
NdFeB	Neodymium iron boron magnet
PM	Permanent magnet
PMASR	Permanent magnet assisted synchronous reluctance
PTO	Power take-off
SPM	Surface permanent magnet
SyRM	Synchronous reluctance machine

I. Introduction

In order to reduce emissions, air pollution, resource waste, and traffic noise, EU government legislation is pushing towards the increase of electric and hybrid vehicle production [1]. This has caused a tectonic change in the automotive industry, both knowledge, and production wise. New traction components like battery, inverter, and electric machine are becoming the most important factors in vehicle design in a matter of cost and packing (component layout within the vehicle) [2], [3]. The battery is usually modular component and inverter is small in size, which means they can in most cases be packed efficiently within the vehicle. On the other hand, the electric machine is usually integrated within some sort of transmission system, which is inherently space consuming [2]. To reduce the size of the drivetrain, electric machine size must be minimized, while efficiency and power density must be kept on the sufficient level.

Currently, due to the inherently high torque and power density, interior rare earth permanent magnet synchronous machines (IPM) are predominantly used for automotive traction (Fig. 2a-b). A notable landmark for IPM machines in automotive hybrid/electric traction was the adoption by both Toyota and Honda, for the first generation of Prius and Insight, respectively [4], [5].

Although the performance benefits are undisputed, the use of rare earth permanent magnet (PM) materials, such as neodymium or dysprosium, has raised concerns in a number of areas. In 2011 and 2012, China reportedly threatened to cut off international supplies of these materials [6], leading to dramatic, though short-term, increase in the material price, increasing as much as 3000% in case of dysprosium [7]. These volatilities have forced the automotive industry to search for the alternative electric machine design, which will either use none or minimal amount of rare earth material.

The alternatives which have not been in recent industry focus are synchronous reluctance machines (SyRM) and its derivatives [8]. These solutions rely on high reluctance torque, thus theoretically needing no PM material in the rotor structure. They have relatively low material costs, low rotor losses and are considered as robust [9], [10]. On the other hand, lack of the permanent magnetic field in the rotor is penalized with lower torque density, lower power factor, and higher torque ripple [11], [12]. This paper will present the theory, state of the art trends in reluctance machine technology and potential applications in vehicle traction. The survey will be performed on pure synchronous reluctance machines (SyRM), and its derivative designs improved by adding permanent magnet material, assisted synchronous reluctance machines (PMASR).

II. SyRM and PMASR theory and design aspects

A. General facts

The stator of the SyRM or PMASR machines is not different from other machine types, therefore, to be able to evaluate and compare different designs, only rotor cross sections will be discussed. Furthermore, this paper will consider only machines for traction applications which are coupled to multi-phase variable frequency drive.

In 1923, Kostko [13] has calculated that if properly designed and manufactured, SyRM performance is comparable with induction machine (IM) of the same volume. During the years SyRM concept evolved from simple squirrel cage, to complex design implementations (Fig. 2e-h), [14], [15].

All of the concepts rely on rotor anisotropic properties designed to produce high reluctance torque. Rotor anisotropy is achieved by large magnetic conductivity differences in d and q axis caused by several flux barriers, and saturation effects in different parts of the rotor core. The purpose of the barriers is to create high resistance path for the flux along the q axis to achieve high saliency ratio, thus producing a high reluctance torque component (Fig. 2e-f). However, barrier bridges and posts are required (at the ends and sometimes in the middle of each barrier) for sustaining rotor structural integrity. A portion of flux flows through these bridges causing a consequent reduction of the torque. Another downside is limited operation in FW area and inherently low power factor (Fig. 3), which requires large variable frequency drive.

If permanent magnets are inserted in each rotor flux barrier (Fig. 2g-h), SyRM is transformed to PMASR. The purpose of the magnets is to saturate barrier bridges, to increase the torque and especially the power factor, which reduces the size of the attached variable frequency drive [11].

Two most commonly used types of PM material are "strong" neodymium (NdFeB) and "weak" ferrite. PM material properties are a function of remanent flux density, coercive force (demagnetization field proportional to demagnetization current) and temperature. Fig. 1 demonstrates operational contrast of NdFeB and ferrite PMs.

At $-40\,^{\circ}$C, NdFeB have remanent flux density around 1,17 T and large coercive force (large current is required for demagnetization) while ferrites have approx. flux density of 0,42 T and smallest coercive force [16]. The main ferrite PM disadvantage is demagnetization at low temperatures [17] which can be an issue ($-40\,^{\circ}$C is the minimal operational temperature of most road vehicles). At high temperatures ($> 150\,^{\circ}$C), similar phenomena happen with NdFeB magnets where rapid reduction of coercive force makes them vulnerable to demagnetization (in practice max. operational temperature of NdFeB magnets is $150\,^{\circ}$C). Here ferrites demonstrate their unique advantage, increasing coercive force with temperature rise, a feature that makes them more resilient to demagnetization. Both PM materials remanent flux density decreases with temperature increase.

Another benefit of ferrite PMs is rotor injection molding, which allows complete filling of the rotor structure (Fig. 2g).

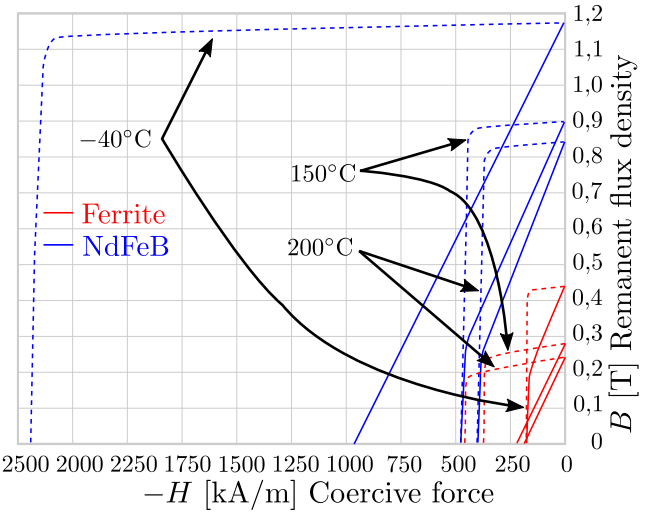

Fig. 1: Comparison of ferrite and NdFeB PM curves at different temperatures [16].

This is not the case with NdFeB PMs, which are produced in specific shapes (Fig. 2h), thus leaving empty space in the rotor flux barriers [18]. This method can further increase power output and reduce losses.

A penalty of SyRM is the inability to have a large number of poles (in practice maximum pole pair number is $p = 2$). Obviously, if the number of poles is increased, magnetic bridges and posts must be reduced to maintain the saliency ratio. This puts pressure on rotor structural integrity. On the other hand, PMASR technology is well suited for high pole-number designs because magnet flux saturates the barrier bridges and posts ($p = 6$ in case of Chevrolet Volt [19]). In this way, bridges can be thicker, which increases structural robustness of the rotor. As an example, in-wheel 12-pole PMASR machine with an external rotor is presented in [20], achieving a 30% reduction of the torque ripple compared with the reference design. In [21], a 16-pole design with a double stator and 3D air-gap concept is presented, improving the efficiency by 5% when compared to a conventional design.

B. Electromagnetic torque

Machines listed in Fig. 2 can be divided in two families. First is alignment torque component dominant group, which includes IPM and SPM machines where PM magnetization direction is aligned with positive d axis (Fig. 2a-d). Second is reluctance torque component dominant group, which includes SyRM and PMASR machines. It is important to emphasize that PMASR PM magnetization direction is opposing positive q axis (Fig. 2g-h), [11].

In general, there are two different rotor paths for the flux (Fig. 2). A distinction of the reluctance machines is a switch of rotor d and q axes in relation to alignment torque dominant family. High permeability path (high magnetic conductivity, d-axis path) is parallel to the flux-barriers. Low permeability path (low magnetic conductivity, q-axis path), is vertical to the rotor flux barriers [11].

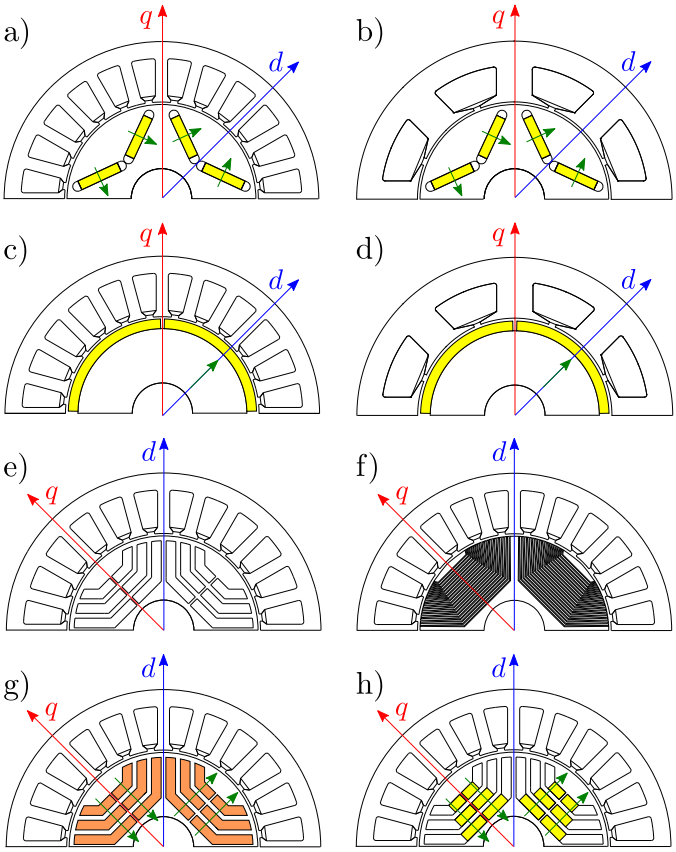

Fig. 2: Example of four pole machine families with corresponding dq axes: IPM with a) distributed and b) concentrated winding stator; SPM with c) distributed and d) concentrated winding stator; e) SyRM; f) AxLam SyRM; g) "weak" PM material PMASR; and h) "strong" PM material PMASR. Green arrows indicate PM magnetization direction.

For both families, torque output consists of alignment and reluctance component and can be written as (1), (3), where L_d, L_q are inductances, i_d, i_q currents in d and q axis, p is the number of pole pairs and λ_m is magnet flux. In case there is no PM material (SyRM, $\lambda_m = 0$), the relation between L_d and L_q will determine the machine torque capability (1). The inductance ratio is reffered as saliency ratio ξ, whose formula depends on the machine family (2), (4), [11].

A high number of cavity layers in each pole combined with a small air-gap typically leads to saliency ratios higher than 3,5 [22]. Lipo and Matsuo report that $\xi = 7 - 8$ can be expected [23], power densities in the order of $5,5{-}7,5$ kW/l can usually be achieved [24], [25]. Apart from the stator and rotor cross-section design, lamination steel selection has an impact on final saliency ratio ($\Delta\xi = \pm 7\%$) [26].

$$\text{Dominant reluctance component machine family} \begin{cases} T_{em} = \frac{3}{2}p\Big[\overbrace{\underbrace{\lambda_m i_d}_{\text{Alignment}} + \underbrace{(L_d - L_q) i_q i_d}_{\text{Reluctance}}}^{\text{PMASR}}\Big] & (1) \\ \xi = L_d / L_q & (2) \end{cases}$$

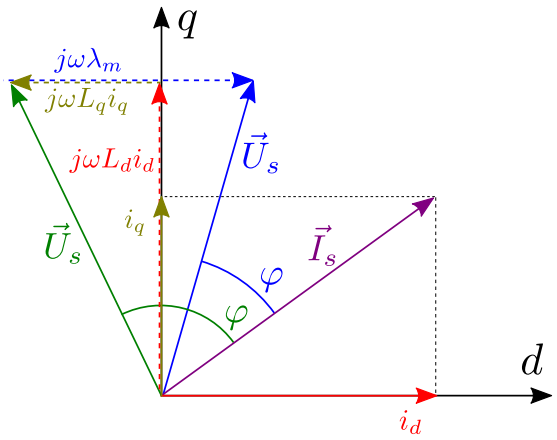

Fig. 3: Voltage phasor diagram of SyRM (green) and PMASR (blue) for a given stator current (stator resistance is neglected $R_s = 0$) [11].

$$\text{Dominant alignment component machine family} \begin{cases} T_{em} = \frac{3}{2}p\Big[\overbrace{\underbrace{\lambda_m i_q}_{\text{Alignment}} + \underbrace{(L_d - L_q) i_q i_d}_{\text{Reluctance}}}^{\text{IPM}}\Big] & (3) \\ \xi = L_q / L_d & (4) \end{cases}$$

C. Combination of PM and reluctance: IPM design plane

Depending on the amount of the rotor PM material and rotor cross-section, IPM and PMASR properties can often overlap and one can argue that IPM is actually PMASR and vice versa. According to the informal rule, if reluctance torque component is greater than 50% of maximum torque at base speed, the machine is considered PMASR. To further differentiate machine families, Soong [27] introduces "IPM design plane" (Fig. 5). From left to right, the plane starts with SyRMs ($\lambda_m = 0$, high saliency, only reluctance torque, Fig. 2e-f) and ends with SPM machines (no saliency $\xi = 1$, only magnet torque, Fig. 2c-d). In between, all IPM machines and PMASR combinations are included.

The optimal IPM design line defines special matches of PM flux and saliency ratios resulting in optimal field weakening (FW) capability, indicating infinite constant power speed range under limited voltage and current constraints (this is valid for ideal machine [27]).

SyRM is out of the optimal design line, whereas PMASR fall into the optimal FW area when the appropriate quantity of magnets is added to a baseline synchronous reluctance design.

D. Rotor laminations assembly

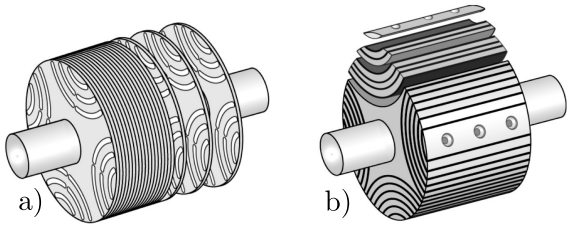

Fig. 4: a) Transversally laminated rotor (TrLam) and b) Axially laminated rotor (AxLam) [28].

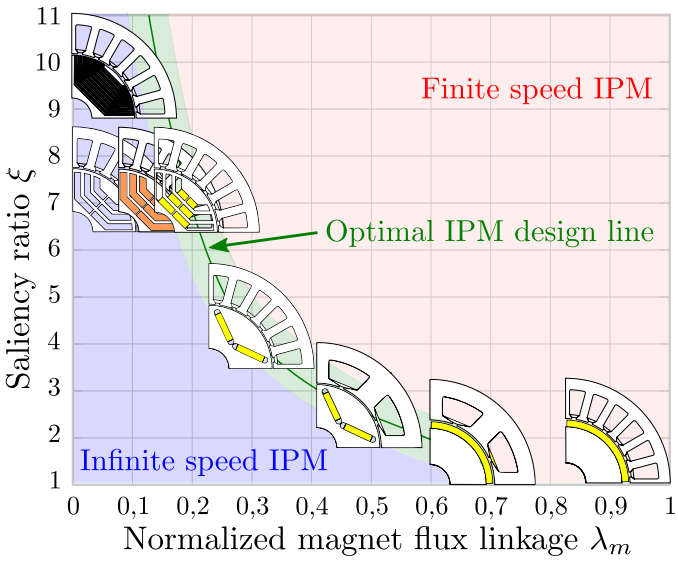

Fig. 5: IPM design plane [11].

SyRM with transversally (conventially) laminated rotor (TrLam) has been proposed in early nineties [14], [29], [30], (Fig. 4a). Machine laminates are produced by punching tool or laser cutting, which removes extra material. The other, non standard production technique is rotor lamination mounting alongside shaft axsis (AxLam, Fig. 4b). Theoretically, this method increases the saliency ratio above the levels achievable with TrLam machines ($\xi > 10$, [19]) using fixed strips of steel separated by thin layers of insulating material [31].

According to Vagati [30], the better suitability of TrLam structure for industrial manufacturing is evident from several aspects: the laminates can be punched with conventional methods, assembly process is straightforward and either constant (in case of PM injection molding), or segmental skewing can be applied on the rotor. In large scale machine manufacturing, stator skewing is normally avoided in favor of using automatic winding devices [32].

On the other hand, AxLam structure theoretically enables high saliency ratio by increasing the number of laminate layers n_l (Fig. 6a). However, this is only true for a two-pole structure ($p = 1$) [30], while for $p > 1$, Bianchi et al. [33] shows that due to the saturation effects, the ideal structure should have a variable ratio between the depths of magnetic and non-magnetic structures where $k_1 < k_2 < k_3$, which reduces saliency ratio (Fig. 6b). To summarize, production difficulties of AxLam rotors are:

- Every laminate segment has different design and size.
- Inter-segment insulation thickness k_i has to vary in-between layers.
- There is no straightforward skewing possibility.
- Rotor circumference needs to be machined after laminate mounting, which can change the material properties and increase iron losses [34].

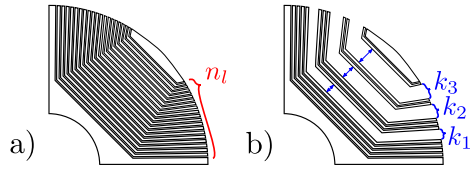

Fig. 6: Sketch of rotor with uniform, and non-uniform distribution of the AxLam laminations.

Due to the rotor magnetic reaction to stator slot harmonics, both TrLam and AxLam options face problems with torque ripple, which makes either rotor or stator skewing a necessity [35]. As mentioned, TrLam rotor can be easily skewed, which is not the case for AxLam rotors, leaving stator skewing as the only option.

Furthermore, when comparing TrLam machine of similar rotor volume, AxLam machines have increased iron losses (Tab. II).

TABLE II. TrLam and AxLam iron loss comparison

Variable	TrLam [36]	AxLam [37]	Unit
n	1500	1500	rpm
p	2	2	-
Rotor diameter	140	136	mm
Stack length	134	160	mm
Power at the shaft @ 1500 rpm	3,6	2,5	kW
Power density @ 1500 rpm	1,7	1,1	kW/l
Iron loss	119	665	W
ξ	8,1	12,5	-

These can be explained in different ways, Maronghiu and Vagati [29] suggest that these losses are due to flux oscillations in stator teeth. A different explanation is given in [37], where losses are caused by rotor eddy currents. Anyway, the additional losses are considerable and represent a further drawback for the AxLam setup [38].

The above-cited reasons are largely sufficient to choose the TrLam rotor type. However, interest on the AxLam type is probably due to the belief that this solution gives a better saliency. This is not correct as comparable anisotropy values are obtained from both rotors, with condition that the pole number is the same. Saliency ratio $\xi = 10$ is a typical, non saturated value for four-pole ($p = 2$) AxLam machine [32].

E. Rotor flux barrier design and number

According to Bianchi [11] and Pellegrino [18], there are multiple parameters which define basic rotor structure in both SyRM and PMASR. Also, asymmetric rotor structures are possible [11], [39], but they are complicated to parametrize and will not be covered in this paper. To simplify the process, several terms are defined (Fig. 7): flux barriers (air cavities in q axis direction), flux carriers (steel guides alternated to flux barriers), barrier bridges (flux barrier ends, whose angular positions at the air-gap are key to minimize torque ripple and

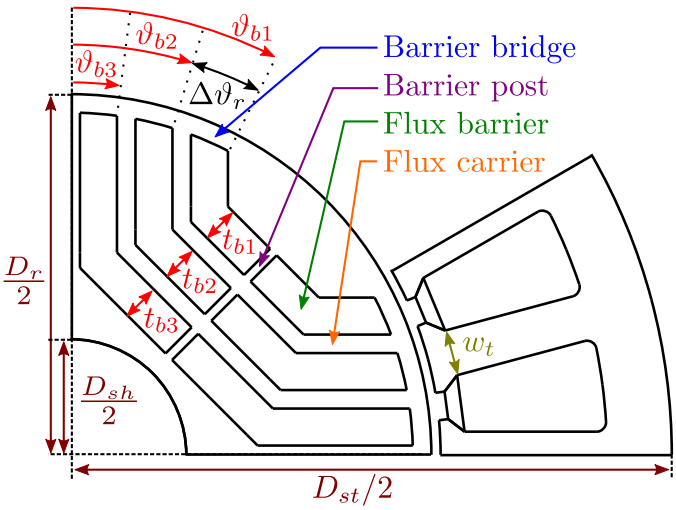

Fig. 7: SyRM/PMASR rotor geometry parameters.

iron losses) and barrier posts (steel reinforcements between flux carriers).

The fundamental rotor design variable is the number of flux barriers (n_l), which can be calculated from (6), where n_r is the number of stator slots (N_s) per pole pair (p), (5). The example machine from Fig. 7 has $N_s = 24$, $p = 2$ meaning $n_l \leq 24/(4 \cdot 2) \leq 3$. In this case, barrier bridges have been designed angularly equidistant (e.g. barrier bridge pitches are: $\vartheta_{b1} : \vartheta_{b2} : \vartheta_{b3} = 3 : 2 : 1$), barrier bridge pitch ($\Delta\vartheta_r$) is considered regular and can be calculated from eq. (7). In practice this does not need to be the case [18]. Obata et al. reports that non uniform pitch distribution can reduce torque ripple [17].

$$n_r = N_s/p \tag{5}$$

$$n_l \leq n_r/4 \tag{6}$$

$$\Delta\vartheta_r = 360/n_r \quad \text{[el. deg.]} \tag{7}$$

A second important set of parameters is barrier thickness distribution (t_{bi}) which correlates to rotor saturation [18]. Referring to Fig. 7, Bianchi defines two coefficients for determining optimal barrier size. $k_{\text{air r}}$ is calculated by eq. (8) where, t_{bi} are the flux barriers thickness, D_r is rotor diameter and D_{sh} is the shaft diameter. Too large $k_{\text{air r}}$ can cause saturation of flux carriers, thus reducing torque output [39]. Second coefficient $k_{\text{air s}}$, is related to the stator geometry (10), where p_s is the stator slot pitch (9) and w_t is tooth width. To keep machine equally saturated coefficients $k_{\text{air r}}$ and $k_{\text{air s}}$ should be kept as equal as possible [11], [23].

$$k_{\text{air r}} = \left[\sum_{i=1}^{n_l} t_{bi}\right] / \left[(D_r - D_{sh})/2\right] \tag{8}$$

$$p_s = (\pi D_{st})/N_s \quad \text{[rad]} \tag{9}$$

$$k_{\text{air s}} = (p_s - w_t)/p_s \tag{10}$$

According to [34], the optimal design of a PMASR has to consider PM demagnetization. To avoid demagnetization, ferrite PMASR flux barriers thickness are recommended to be the same along their length. Alternatively, short NdFeB magnets may be placed on the bottom of rotor flux barriers.

F. Barrier bridges and posts reduction methods

In practice, barrier bridge (Fig. 8c) and post (Fig. 8b) thickness is minimized to reduce torque ripple and losses, while keeping the structural integrity of the rotor.

After a preliminary design is done, mechanical structural finite element method (FEM) and fatigue analysis have to be performed. If rotor design is angularly symmetrical, only one rotor pole has to be considered. Rotor material properties are key inputs for mechanical analysis. In case of SyRMs, only laminate steel data is required (Fig. 8d). PMASR calculation requires additional PM mechanical data. PMs are considered to be a part of the rotor mass without any load-carrying capacity. To avoid calculation issues, a good practice is to "glue" PMs to the laminate surface within FEM software.

Static resistance (one operating point, i.e. at 5220 rpm) to centrifugal load is assessed by using a classic approach based on the average stress over the reduced section [40]. Vibrations and shaft dynamical forces are neglected. The analysis result is often presented in a form of Von Misses stress distribution (Fig. 8b-c), and maximum material displacement (Fig. 8a). The common way of determining design quality is the factor of safety (FOS), which measures how much load will the designed part actually be able to withstand (Fig. 8e). FOS is calculated by equation (11), where σ_{max} is maximal simulated Von Misses stress, and $\sigma_{0,2}$ is yield strength at 0,2 strain, which represents material elastic deformation limit. Typically, it is required that the maximum rotor stress calculated at maximum over-speed ($1,2 \cdot n_{max}$ [41]) is approximately 2 times lower than the nominal yield strength of the rotor lamination (FOS ≈ 2).

$$\text{FOS} = \sigma_{0,2}/\sigma_{\text{max}} \tag{11}$$

Fatigue analysis is performed to assess the iron bridge lifetime, resulting from cyclic loading. It requires careful considerations due to the reduced value of the tip radii at the corners of the flux barriers and cavities. FEM mesh needs to be sufficiently dense in these areas for a valid result. Extreme operating conditions have to be considered, consisting of repeated start and stop cycles (zero to maximum speed, [40]).

Apart from barrier bridges and posts minimization through electromagnetic and mechanical optimization, Reddy et al. [25], [42] propose a rotor retaining sleeve. The sleeve reduces laminate stress, allowing smaller bridge dimensions. Another approach in [24] proposes a magnetic material which allows the selective introduction of non-magnetic regions in the barrier bridges and posts. This is achieved by local heat treatment of laminations.

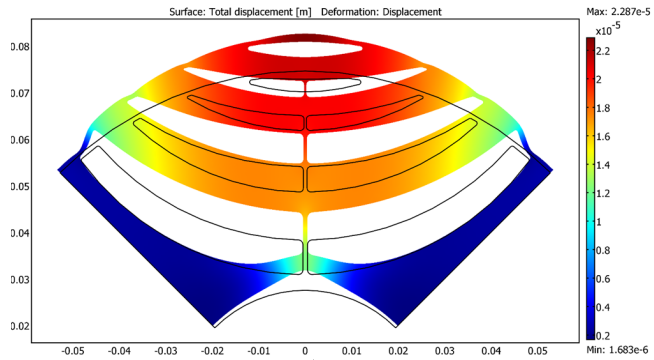

a)

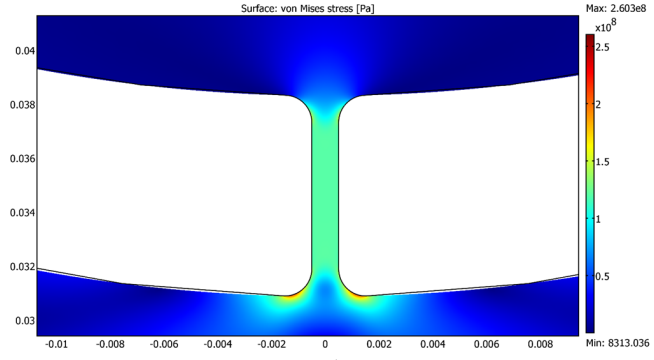

b)

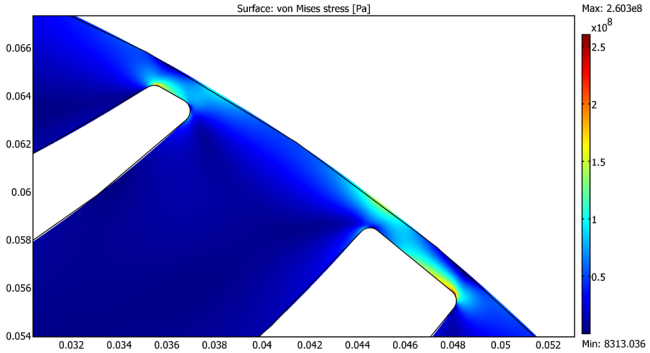

c)

d)

Name	Variable	Value	Unit
Laminate steel	M530-50A	-	-
Density	ρ	7858	kg/m^3
Yield strength	$\sigma_{0,2}$	295	MPa
Young module	E	$2 \cdot 10^{11}$	Pa
Poisson ratio	υ	0,29	-
Thermal expansion coefficient	α	$1,2 \cdot 10^{-5}$	1/K

e)

n [rpm]	σ_{max} [MPa]	FOS
5220	258,4	1,14
4200	167,3	1,76
3600	122,9	2,4

Fig. 8: a) Exaggerated pole displacement; b) Barrier post stress detail; c) Barrier bridge stress detail; d) Material properties table; e) FOS calculation table;

G. Machine design and rotor optimization

The machine design is performed in several steps. Each step usually requires multiple iterations until satisfying results are obtained [43], [44].

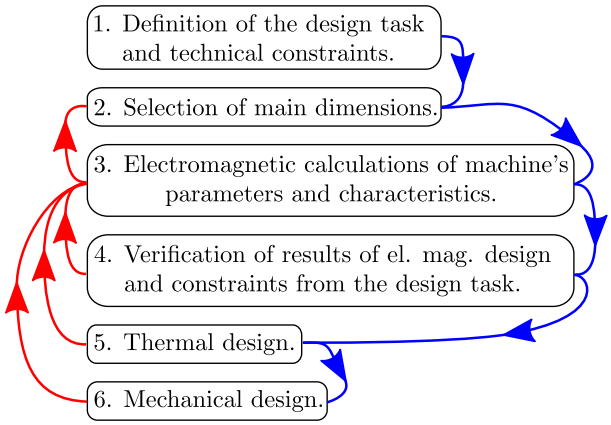

Fig. 9: Electric machine design algorithm example [43].

If the machine volume envelope is defined, the performance will be determined by electromagnetic and thermal design (cooling capability) [45]. There are two approaches to electromagnetic and thermal design. First is lumped parameter modeling which allows fast iterative computations with a precision penalty (especially in case of thermal design). The second approach is based on FEM where electromagnetic design can be downsized to a 2D problem, while precise thermal modeling requires 3D computational fluid dynamics (CFD) simulations (the penalty is prolonged simulation time). In practice, a combination of both approaches together with empiric methods yields acceptable results [45].

This paper concentrates only on SyRM and PMASR electromagnetic performance which is mostly determined by rotor topology optimization. According to Pellegrino [18], a golden rule for a good PMASR is a SyRM baseline which is then gradually modified towards optimal design.

As previously stated, there are many parameters (Fig. 7) which define the rotor cross section and machine performance. In example, Liu et al. in [46] reports that PMASR efficiency can be improved by 6% with optimal magnet placement. Finding the optimal parameters is a classic Pareto multi-objective optimization problem [47].

Some of the optimization methods are genetic algorithms, differential evolution (DE), and simulated annealing [48]. DE is stochastic evolutionary optimization algorithm [49], [50], [51], which gives the best results in terms of convergence time and repeatability [48]. Together with the machine parameters, the optimization algorithm requires one or several goal functions, which provide a parameter selection boundary (i.e. maximize torque [52], minimize torque ripple, minimize material cost, etc.).

In comparison to other machine types, SyRM and PMASR

can have a large number of rotor parameters. Reduction of parameter numbers will simplify the design and reduce computational time. The recommended compromise between output performance and computational time is to limit the number of degrees of freedom for two [53], or three [54] per rotor barrier.

III. Commercial applications

A. Industry

The first notable modern industrial commercialization of the SyRM was done by ABB in 2012. As an example, 90 kW machine measured nominal efficiency of 96,1% @ $\cos\varphi = 0,73$, illustrating both the strengths and challenges of this technology [55], [11]. Today, in addition to ABB, various manufacturers such as Kaiser Motoren, REEL, SIEMENS, and Končar MES provide solutions in the $0,55 - 315$ kW range [9], [56]. The main reason SyRM designs came in to spotlight is the introduction of the new IEC 60034-30-1 standard with harsher efficiency constraints. Introduction of IE4 super-premium efficiency class [57], and better efficiency in comparison to IMs, makes SyRM attractive for industrial use.

B. Automotive traction

Up to today, SyRM has not been commercialized in large scale automotive traction. One of the rare examples adapted for the electric vehicle is Ricardo 85 kW 6ph SyRM [58]. MotorBrain project [59] has investigated an inverter power module integration with SyRM stator for automotive application. The project resulted in 97,6% efficiency inverter and 93,6% efficiency 6ph 60 kW SyRM (overall system 91,6%).

The conclusion is that the current low volume production of electric/hybrid in comparison to internal combustion vehicles still favors the use of IPM machines.

On the other hand, PMASR machines are a direct competitor to IPM machines and have already been commercialized in the automotive industry. The example is second generation Chevrolet Volt which uses ferrite [19] and BMW i3 which mounts NdFeB magnets [60], [61], [8]. Second-generation Toyota Prius machine [62] is slightly on the side of the IPM family (alignment torque component at base speed is slightly above 50% of maximum torque).

C. Ship propulsion and freight traction

SyRM is considered to be a direct competitor of IMs which are often used in railway and ship propulsion. This has been confirmed by [63], concluding that both IM and SyRM have similar electric, magnetic, and thermal performance, with SyRM having lower rotor losses. Germishuizen et al. emphasize that SyRM compared to IM have lower stator winding temperature rise, which allows an increase of the power rating by 5 - 10% [64]. All authors agree that the main drawbacks of the SyRM solution is low torque in FW range and inherently large variable frequency drive.

Although SyRM in relation to PMASR has a lower power factor, its main benefit is high overload capability, without any demagnetization problems [65].

D. Commercial vehicles

To power the special equipment (cranes, refuse system, refrigerators, etc.), the commercial vehicle must be fitted with an extra means of a power supply, a power take-off (PTO). One or more PTOs transfer power from the engine to drive attachments or load handling equipment. The PTO provides a mechanical link (output shaft) towards load (usually some sort of hydraulic system) with most of the systems having power demand < 80 kW [66]. Historically, the PTO output shaft has been a part of the combustion engine or transmission (Fig. 10a-d). With recent commertial vehicle electrification trends [67], [68], PTO will most likely be an extra electric machine mounted on the vehicle chassis (Fig. 10e-h). The PTO machine will be powered via inverter attached to the traction battery.

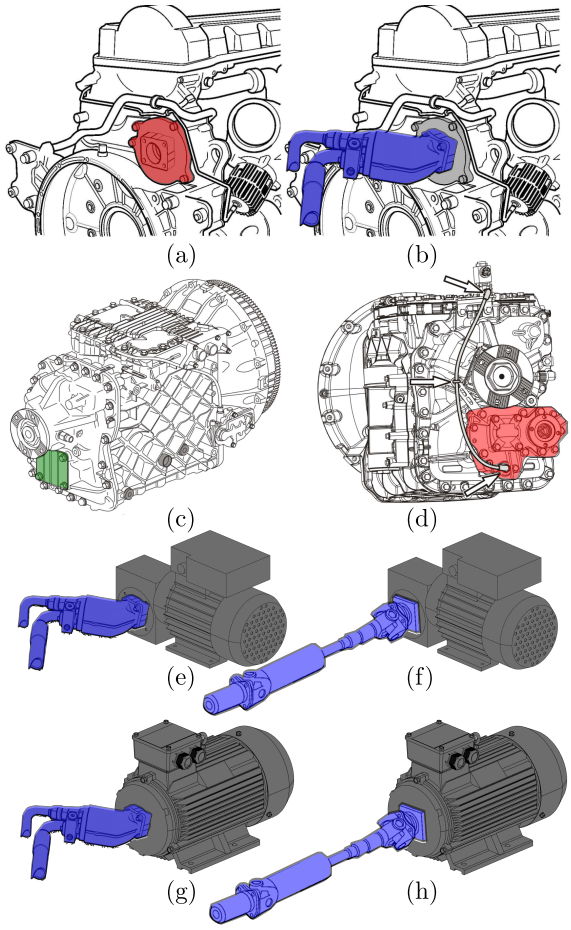

Fig. 10: a) Diesel engine rear PTO mount; b) diesel engine with mounted hydraulic pump; c) Transmission with direct PTO mount; d) transmission with geared PTO [69]; geared PTO propelling hydraulic pump e) and universal joint shaft f); direct PTO propelling hydraulic pump g) and universal joint shaft h).

IV. Theoretical SyRM and PMASR performance

This section examines theoretical limitations of the SyRM, and ferrite and NdFeB PMASR for different saliency ratios ($\xi = 4 - 10$). The calculations are assuming lossless linear machine ($R_s = 0$), driven from inverter with limited voltage and current [16], [70], [71]. All machines have the same

cross section for the given saliency ratio (L_d is fixed and $L_q = L_d/\xi$). In case of SyRM, magnet flux is zero, in ferrite PMASR $\lambda_m = 0,095$ [11], and NdFeB PMASR $\lambda_m = 2,5 \cdot 0,095 = 0,2375$ [65]. Theoretical maximum performance has been calculated using Matlab based MTPA optimization method described in [72]. All inputs variables are listed in Table III in normalized form.

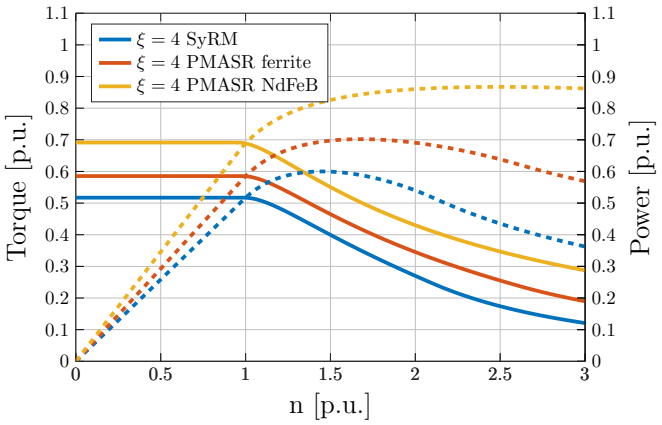

Fig. 11: Performance comparison of SyRM, ferrite and NdFeB PMASR at fixed saliency ratio.

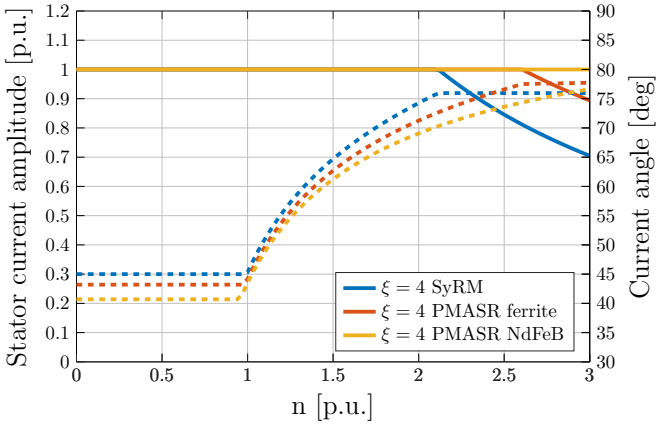

Fig. 12: Current amplitude and angle comparison of SyRM, ferrite and NdFeB PMASR at fixed saliency ratio.

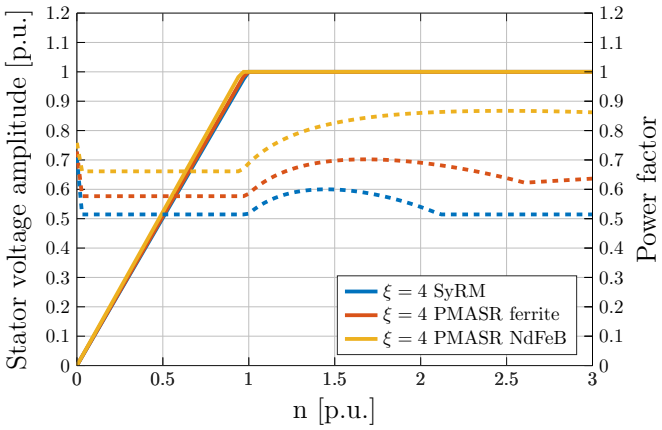

Fig. 13: Voltage amplitude and power factor comparison of SyRM, ferrite and NdFeB PMASR at fixed saliency ratio.

A. *Comparison at fixed saliency*

If saliency ratio is kept constant at $\xi = 4$, by adding PM material, base torque increases from 0,5 to 0,6 (ferrite PMASR) and 0,7 (NdFeB PMASR) (Fig. 11). There is a large power difference in FW operation. SyRM and ferrite PMASR power rapidly drops, while NdFeb PMASR remains constant up to the maximum speed. Such NdFeb PMASR behavior is due to the fact that the λ_m has been chosen to achieve the characteristic current I_c close to the maximum inverter current $I_{\text{s max}}$. The characteristic current (also known as short circuit current) is defined as $I_c = \lambda_m/L_q$ [11].

Fig. 12 confirms that inverter is operating on the current limit (current amplitude is always 1 in case of NdFeb PMASR) and voltage limit is not reached. Prior to FW, SyRM current angle is fixed to $45°$ which follows constant torque hyperbola vertex. Adding the PMs reduces the angle which is always $< 45°$ in case of PMASRs. As SyRM and ferrite PMASR reach voltage limit, the current amplitude reduces and angle becomes constant.

Fig. 13 shows another important effect of adding PMs, the increase of the power factor in the whole operating region. The power factor increases with PM strength and it is always higher than in the case of SyRM machine. The power factor improvement is more beneficial as the speed increases. In the case of PMASR solution, it means that the size of the inverter could be decreased for the same performance requirement.

TABLE III. Parameters of SyRM and ferrite/NdFeB PMASR

Variable	[SyRM; Fe PMASR; NeFeB PMASR]	Unit
ξ	[4 6 8 10]	-
λ_m	[0; 0,095; 0,2375;]	-
L_d	1,379	-
L_q	L_d/ξ	-
p	2	-
$\omega_{\text{el base}}$	1	-
$U_{\text{s max}}$	1	-
$I_{\text{s max}}$	1	-
n_{base}	$\omega_{\text{el base}} \cdot 30/(\pi p)$	p.u.
U_{base}	$U_{\text{s max}}$	p.u.
I_{base}	$I_{\text{s max}}$	p.u.
S_{base}	$3/2 \cdot I_{\text{base}} \cdot U_{\text{base}}$	p.u.
Z_{base}	$U_{\text{base}}/I_{\text{base}}$	p.u.
L_{base}	$Z_{\text{base}}/\omega_{\text{el base}}$	p.u.
T_{base}	$S_{\text{base}}/(p \cdot \omega_{\text{el base}})$	p.u.
ψ_{base}	$U_{\text{base}}/\omega_{\text{el base}}$	p.u.

B. *Saliency ratio variation effects to maximum performance*

Higher saliency ratio by large margin improves SyRM (Fig. 14) and ferrite PMASR (Fig. 15) performance in FW range. NdFeB PMASR (Fig. 16) has satisfactory performance trough whole FW range. Table IV summarizes the performance at $n = 1, 5$.

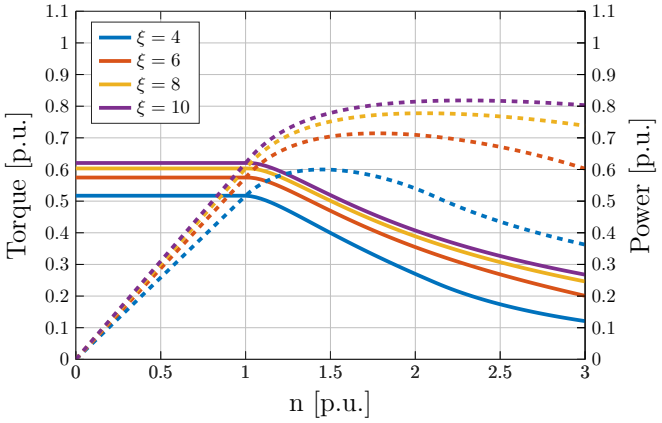

Fig. 14: Performance curves of SyRM for $\xi = 4 - 10$

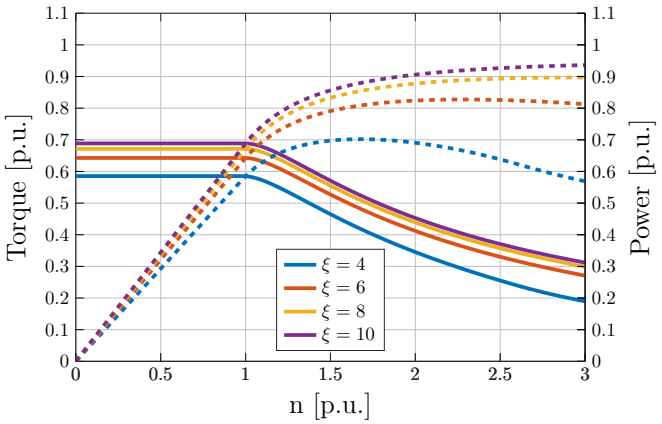

Fig. 15: Performance curves of ferrite PMASR for $\xi = 4 - 10$

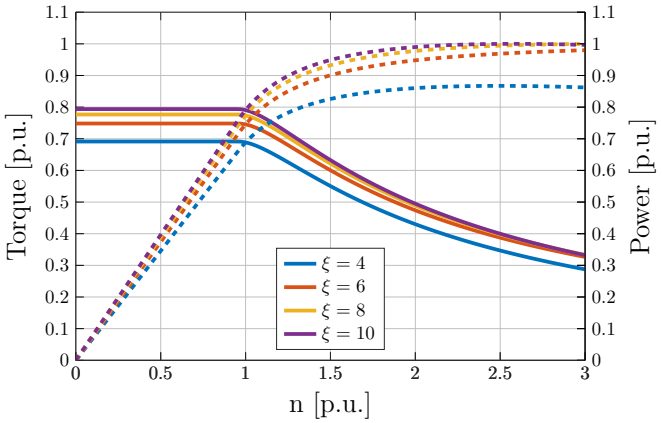

Fig. 16: Performance curves of NdFeB PMASR for $\xi = 4 - 10$

TABLE IV. Comparison of peak performance values of SyRM, ferrite and NdFeB PMASR at $n = 1, 5$ and $\xi = 4 - 10$.

ξ	n	T_{SyRM}	T_{Fe}	T_{NdFeB}	P_{SyRM}	P_{Fe}	P_{NdFeB}
4	1,5	0,40	0,46	0,55	0,60	0,70	0,83
6	1,5	0,47	0,52	0,60	0,71	0,79	0,90
8	1,5	0,50	0,55	0,62	0,75	0,83	0,93
10	1,5	0,52	0,57	0,63	0,78	0,86	0,95

V. Conclusion

The paper has covered the SyRM and PMASR theory, design aspects, and prospective commercial applications. Special attention has been addressed to differentiate reluctance and alignment torque component dominant families, and to list all PM machine theory equations and principles in one paper.

In comparison to the alignment torque component dominant machine family, reluctance machines have a large number of rotor parameters, which increases the duration of the electromagnetic design process and create issues for rotor mechanical analysis. Nevertheless, when properly designed, reluctance machines can be robust and contain no rare earth PM material, making them attractive from the cost point of view.

Replacing high-performance IPMs with rare-earth-free machines poses difficult challenges above all in terms of power density. A number of drawbacks, such as the demagnetization risk of the ferrite magnets at low temperatures, and reduced rotor mechanical strength, should be taken into account for the successful introduction of the technology.

Considering all available information, reluctance machine technology seems promising. However, each particular application has to be analyzed to find out which design variant (SyRM or PMASR, etc.) should be used.

VI. Acknowledgment

This work was partially supported by the Croatian Science Foundation under the project IP-2018-01-5822 - HYDREL.

Appendix A
Summary of Figures and Equations to Differentiate Reluctance and Alignment Torque Component Dominant Families

A detailed review of the literature has confirmed that reluctance and alignment torque component machine families are still not strictly separated in the scientific community. Depending on the author, different dq reference frame approaches can be used, leading to PMASRs being described with IPM equations. This is mathematically correct, but differs from dq frame convention described in section II-A. This appendix summarizes the approaches used for different machine families. Equations valid for both families are listed in (12-14), while current and voltage constraint, constant torque hyperbolas, torque and saliency ratio equations are listed in Fig. 17.

$$\underbrace{\begin{bmatrix} u_d \\ u_q \end{bmatrix}}_{\boldsymbol{u_s}} = R_s \underbrace{\begin{bmatrix} i_d \\ i_q \end{bmatrix}}_{\boldsymbol{i_s}} + \omega_e \begin{bmatrix} 0 & -1 \\ 1 & 0 \end{bmatrix} \underbrace{\begin{bmatrix} \psi_d \\ \psi_q \end{bmatrix}}_{\boldsymbol{\psi_s}} + \underbrace{\begin{bmatrix} \dot{\psi}_d \\ \dot{\psi}_q \end{bmatrix}}_{\dot{\boldsymbol{\psi}}_{\boldsymbol{s}}} \tag{12}$$

$$|\boldsymbol{u_s}|^2 = u_d^2 + u_q^2 \tag{13}$$

$$\left(\frac{|\boldsymbol{u_s}|}{\omega_e}\right)^2 = \psi_d^2 + \psi_q^2 \tag{14}$$

Dominant reluctance component machine family

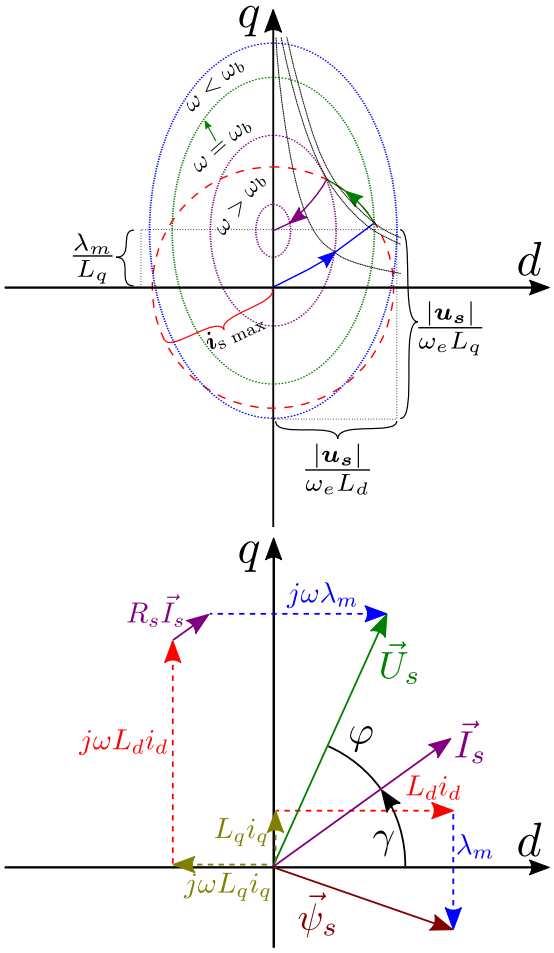

$$T_{em} = \frac{3}{2}p\left[\overbrace{L_d i_d}^{\psi_d} i_q - \overbrace{(L_q i_q - \lambda_m)}^{\psi_q} i_d\right]$$

$$= \frac{3}{2}p\left[\overbrace{\lambda_m i_d + \underbrace{(L_d - L_q) i_q i_d}_{\text{SRM}}}^{\text{PMASR}}\right]$$

$$\xi = L_d/L_q$$

$$L_d >> L_q$$

$$i_q \geq 0$$

$$\left(\frac{|u_{s\ max}|}{\omega_e}\right)^2 \geq L_d^2 i_d^2 + L_q^2 (i_q - \lambda_m/L_q)^2$$

$$\left(\frac{|u_{s\ max}|}{\omega_e L_d L_q}\right)^2 \geq \frac{i_d^2}{L_q^2} + \frac{(i_q - \lambda_m/L_q)^2}{L_d^2}$$

$$1 \geq \frac{i_d^2}{\left(\frac{|u_{s\ max}|}{\omega_e L_d}\right)^2} + \frac{(i_q - \lambda_m/L_q)^2}{\left(\frac{|u_{s\ max}|}{\omega_e L_q}\right)^2}$$

Dominant alignment component machine family

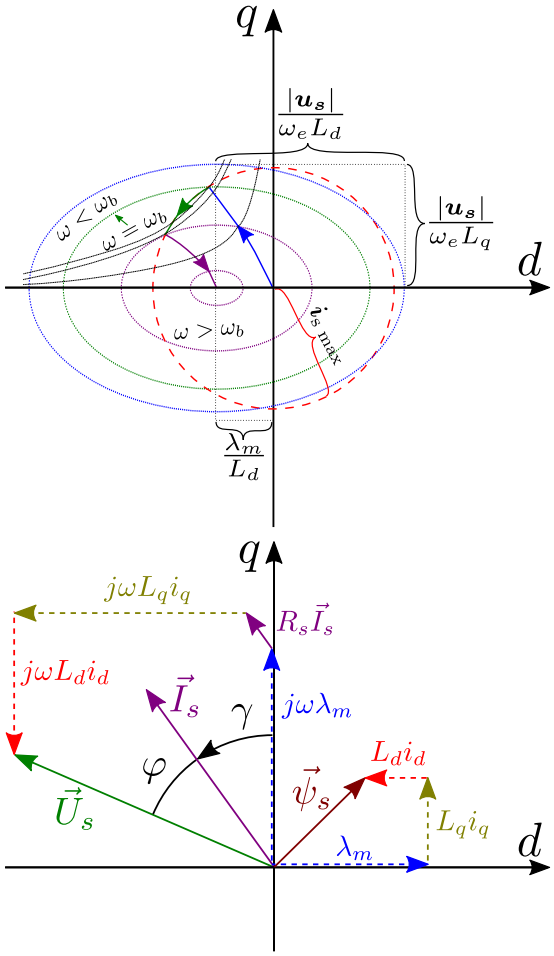

$$T_{em} = \frac{3}{2}p\left[\overbrace{(L_d i_d + \lambda_m)}^{\psi_d} i_q - \overbrace{L_q i_q}^{\psi_q} i_d\right]$$

$$= \frac{3}{2}p\left[\overbrace{\underbrace{\lambda_m i_q}_{\text{SPM}} + (L_d - L_q) i_q i_d}^{\text{IPM}}\right]$$

$$\xi = L_q/L_d$$

$$L_q \geq L_d$$

$$i_d \leq 0$$

$$\left(\frac{|u_{s\ max}|}{\omega_e}\right)^2 \geq L_d^2 (i_d + \lambda_m/L_d)^2 + L_q^2 i_q^2$$

$$\left(\frac{|u_{s\ max}|}{\omega_e L_d L_q}\right)^2 \geq \frac{(i_d + \lambda_m/L_d)^2}{L_q^2} + \frac{i_q^2}{L_d^2}$$

$$1 \geq \frac{(i_d + \lambda_m/L_d)^2}{\left(\frac{|u_{s\ max}|}{\omega_e L_d}\right)^2} + \frac{i_q^2}{\left(\frac{|u_{s\ max}|}{\omega_e L_q}\right)^2}$$

Fig. 17: Voltage and current constrains, voltage vector diagrams and equations for dominant reluctance torque component family (left) and dominant alignment torque component family (right).

REFERENCES

[1] European Environment Agency, "Electric Vehicles in Europe," p. 60, 2016. [Online]. Available: https://www.eea.europa.eu/publications/electric-vehicles-in-europe

[2] M. Eshani, Y. Gao, S. Gay, and A. Emadi, *Modern electric, hybrid electric and fuel cell vehicles 2nd. Edition*. CRC Press, 2010.

[3] H. Z. De La Parra, F. Magnussen, and S. Bosga, "Challenges for electric machines and power electronics in automotive applications," *International Conference on Ecological Vehicles and Renewable Energies,(EVER'09)*, pp. 1–9, 2009.

[4] J. S. Hsu, C. Ayers, and C. Coomer, "Report on Toyota/Prius motor design and manufacturing assessment," Tech. Rep., 2010. [Online]. Available: https://goo.gl/fuEtvS

[5] A. Kabasawa and K. Takahashi, "Development of the IMA motor for the V6 hybrid midsize sedan," *SAE transactions*, vol. 2005, no. 724, p. 8, 2005.

[6] K. Bourzac, "The Rare-Earth Crisis," 2011. [Online]. Available: https://www.technologyreview.com/s/423730/the-rare-earth-crisis/

[7] J. Rowlatt, "Rare earths: Neither rare, nor earths," 2014. [Online]. Available: http://www.bbc.com/news/magazine-26687605

[8] U. Departent of Energy, "Annual Progress Report Electric Drive Technologies Program," Tech. Rep. July, 2011.

[9] J. R. Riba, C. López-Torres, L. Romeral, and A. Garcia, "Rare-earth-free propulsion motors for electric vehicles: A technology review," *Renewable and Sustainable Energy Reviews*, vol. 57, pp. 367–379, 2016.

[10] S. Estenlund, M. Alaküla, and A. Reinap, "PM-less machine topologies for EV traction: A literature review," *2016 International Conference on Electrical Systems for Aircraft, Railway, Ship Propulsion and Road Vehicles and International Transportation Electrification Conference, ESARS-ITEC 2016*, 2016.

[11] G. Pellegrino, T. M. Jahns, N. Bianchi, W. L. Soong, and F. Cupertino, *The Rediscovery of Synchronous Reluctance and Ferrite Permanent Magnet Motors Tutorial Course Notes*. Springer, 2016.

[12] P. Duck, J. Jurgens, and B. Ponick, "Calculation of Synchronous Reluctance Machines Used as Traction Drives," *2015 IEEE Vehicle Power and Propulsion Conference, VPPC 2015 - Proceedings*, pp. 0–4, 2015.

[13] J. K. Kostko, "Polyphase reaction synchronous motors," *Journal of the American Institute of Electrical Engineers*, vol. 42, no. 11, pp. 1162–1168, 1923.

[14] A. Fratta and A. Vagati, "A Reluctance Motor Drive for High Dynamic Performance Applications," *IEEE Transactions on Industry Applications*, vol. 28, no. 4, pp. 873–879, 1992.

[15] D. Staton, T. Miller, and S. Wood, "Maximising the saliency ratio of the synchronous reluctance motor," *IEE Proceedings B Electric Power Applications*, vol. 140, no. 4, pp. 249–259, 1993.

[16] D. Žarko, "Modern electric machine design methods course materials: "Design of PMSM series motor"," 2014.

[17] M. Obata, S. Morimoto, M. Sanada, and Y. Inoue, "Performance of PMASynRM with ferrite magnets for EV/HEV applications considering productivity," *IEEE Transactions on Industry Applications*, vol. 50, no. 4, pp. 2427–2435, 2014.

[18] G. Pellegrino, "Permanent Magnet Machine Design and Analysis with a Focus to Flux-switching PM and PM-assisted Synchronous Reluctance Machines Part II: PM-assisted Synch Rel Machines," *ICEM*, 2016.

[19] T. Jahns, "Getting Rare-Earth Magnets Out of EV Traction Machines: A review of the many approaches being pursued to minimize or eliminate rare-earth magnets from future EV drivetrains," *IEEE Electrification Magazine*, vol. 5, no. 1, pp. 6–18, 2017.

[20] S. S. Reddy Bonthu, A. Arafat, and S. Choi, "Comparisons of Rare-Earth and Rare-Earth-Free External Rotor Permanent Magnet Assisted Synchronous Reluctance Motors," *IEEE Transactions on Industrial Electronics*, vol. 64, no. 12, pp. 9729–9738, 2017.

[21] K. Kondo, S. Kusase, T. Maekawa, and K. Hanada, "A new PM-assisted synchronous reluctance motor with three-dimensional trench air gap," *IEEE Transactions on Industry Applications*, vol. 50, no. 4, pp. 2485–2492, 2014.

[22] C. T. Liu, H. Y. Chung, and S. Y. Lin, "On the Electromagnetic Steel Selections and Performance Impact Assessments of Synchronous Reluctance Motors," *IEEE Transactions on Industry Applications*, vol. 53, no. 3, pp. 2569–2577, 2017.

[23] T. Lipo and T. Matsuo, "Rotor Design Optimization of Synchronous Reluctance Machine," *IEEE Transactions on Energy Conversion*, vol. 9, no. 2, pp. 359–365, 1994.

[24] P. B. Reddy, A. M. El-Refaie, S. Galioto, and J. P. Alexander, "Design of Synchronous Reluctance Motor Utilizing Dual-Phase Material for Traction Applications," *IEEE Transactions on Industry Applications*, vol. 53, no. 3, pp. 1948–1957, 2017.

[25] A. El-Refaie, T. Raminosoa, P. Reddy, S. Galioto, D. Pan, K. Grace, J. Alexander, and K. K. Huh, "Comparison of traction motors that reduce or eliminate rare-earth materials," *IET Electrical Systems in Transportation Research*, vol. 7, no. 3, pp. 207–214, 2016.

[26] M. N. Ibrahim, P. Sergeant, and E. M. Rashad, "Synchronous Reluctance Motor Performance Based on Different Electrical Steel Grades," *IEEE Transactions on Magnetics*, vol. 51, no. 11, pp. 1–4, 2015.

[27] W. L. Soong and T. J. E. Miller, "Field-weakening performance of brushless synchronous AC motor drives," *IEEE Elec. Power Appl.*, pp. 331–340, 1994.

[28] T. Fukami, M. Momiyama, K. Shima, R. Hanaoka, and S. Takata, "Steady-State Analysis of a Dual-Winding Reluctance Generator With a Multiple-Barrier Rotor," *IEEE Transactions on Energy Conversion*, vol. 23, no. 2, pp. 492–498, 2008.

[29] I. Marongiu and A. Vagati, "Improved modelling of a distributed anisotropy synchronous reluctance machine," *IEEE Industry Applications Society Annual Meeting*, pp. 239–243, 1991.

[30] A. Vagati, "The synchronous reluctance solution: a new alternative in AC drives," *Proceedings of IECON'94 - 20th Annual Conference of IEEE Industrial Electronics*, vol. 1, pp. 1–13, 1994.

[31] W. L. Soong, D. A. Staton, and T. J. E. Miller, "Design of a New Axially-laminated Interior Permanent Magnet Motor," *IEEE Transactions on Industry Applications*, vol. 31, no. 2, pp. 358–367, 1995.

[32] R. R. Moghaddam, F. Magnussen, and C. Sadarangani, "Synchronous Reluctance Machine (SynRM) Design," Ph.D. dissertation, KTH, 2007.

[33] N. Bianchi and B. J. Chalmers, "Axially laminated reluctance motor: Analytical and finite-element methods for magnetic analysis," *IEEE Transactions on Magnetics*, vol. 38, no. 1 II, pp. 239–245, 2002.

[34] I. Boldea and L. Tutelea, *Reluctance Electric Machines Design and Control*. CRC Press, 2019, vol. 91.

[35] A. Vagati, M. Pastorelli, G. Franceschini, and S. C. Petrache, "Design of low-torque-ripple synchronous reluctance motors," *IEEE Transactions on Industry Applications*, vol. 34, no. 4, pp. 758–765, 1998.

[36] M. J. Kamper, F. S. Van Der Merwe, and S. Williamson, "Direct Finite Element Design Optimisation of the Cageless Reluctance Synchronous Machine," *IEEE Transactions on Energy Conversion*, vol. 11, no. 3, pp. 547–553, 1996.

[37] B. J. Chalmers and L. Musaba, "Design and field-weakening performance of a synchronous reluctance motor with axially laminated rotor," *IEEE Transactions on Industry Applications*, vol. 34, no. 5, pp. 1035–1041, 1998.

[38] A. Vagati, M. Pastorelli, P. Guglielmi, and A. Canova, "Synchronous reluctance motor based sensorless drive for general purpose application," Politecnico di Torino, Torino, Tech. Rep., 2002.

[39] M. Ferrari, N. Bianchi, and E. Fornasiero, "Analysis of rotor saturation in synchronous reluctance and PM-assisted reluctance motors," *IEEE Transactions on Industry Applications*, vol. 51, no. 1, pp. 169–177, 2015.

[40] M. Barcaro, G. Meneghetti, and N. Bianchi, "Structural analysis of the interior PM rotor considering both static and fatigue loading," *IEEE Transactions on Industry Applications*, vol. 50, no. 1, pp. 253–260, 2014.

[41] IEEE-SA Standards Board, "IEEE Standard for Rotating Electric Machinery for Rail and Road Vehicles," IEEE Power Engineering Society, Tech. Rep., 2000.

[42] P. B. Reddy, K. Grace, and A. El-Refaie, "Conceptual design of sleeve rotor synchronous reluctance motor for traction applications," *Proceedings - 2015 IEEE International Electric Machines and Drives Conference, IEMDC 2015*, vol. 10, pp. 195–201, 2016.

[43] D. Žarko, "Design of Synchronous Permanent Magnet Motors Manual," Zagreb, p. 88, 2016.

[44] S. Taghavi and P. Pillay, "A Sizing Methodology of the Synchronous Reluctance Motor for Traction Applications," *IEEE Journal of Emerging and Selected Topics in Power Electronics*, vol. 2, no. 2, pp. 329–340, 2014.

[45] D. Stanton and M. Popescu, "Motor-CAD Manual V11," 2018.

[46] H. C. Liu, I. G. Kim, Y. J. Oh, J. Lee, and S. C. Go, "Design of Permanent Magnet-Assisted Synchronous Reluctance Motor for Max-

imized Back-EMF and Torque Ripple Reduction," *IEEE Transactions on Magnetics*, vol. 53, no. 6, pp. 2015–2018, 2017.
[47] P. Di Barba, *Multiobjective Shape Design in Electricity and Magnetism*. Springer, 2010.
[48] F. Cupertino, G. Pellegrino, and C. Gerada, "Design of Synchronous Reluctance Machines with Multi-Objective Optimization Algorithms," *IEEE Transactions on Industry Applications*, vol. 50, no. c, pp. 3617–3627, 2014.
[49] S. Stipetić, "Optimization of electromagnetic design of synchronous permanent magnet motor series," Ph.D. dissertation, Zagreb, 2014.
[50] R. Storn and K. Price, "Differential Evolution – A Simple and Efficient Heuristic for Global Optimization over Continuous Spaces," *Journal of Global Optimization*, vol. 11, pp. 341–359, 1997.
[51] S. Das and P. N. Suganthan, "Differential Evolution: A Survey of the State of the Art," *IEEE Transactions on Evolutionary Computation*, no. May 2014, pp. 1–28, 2010.
[52] D. Zarko, D. Ban, and T. Lipo, "Design optimization of interior permanent magnet (IPM) motors with maximized torque output in the entire speed range," *2005 European Conference on Power Electronics and Applications*, no. 1, pp. 1–10, 2005.
[53] G. Pellegrino, F. Cupertino, and C. Gerada, "Automatic Design of Synchronous Reluctance Motors Focusing on Barrier Shape Optimization," *IEEE Transactions on Industry Applications*, vol. 51, no. 2, pp. 1465–1474, 2015.
[54] M. Gamba, G. Pellegrino, and F. Cupertino, "Optimal Number of Rotor Parameters for the Automatic Design of Synchronous Reluctance Machines," *Proceedings - 2014 International Conference on Electrical Machines, ICEM 2014*, pp. 1334–1340, 2014.
[55] ABB, "DOLSynRM Concept introduction up to IE5 efficiency," p. 5, 2015. [Online]. Available: https://bit.ly/2PwSuym
[56] REEL, "REEL SuPremE® – The IE5* magnet-free synchronous reluctance motor datasheet," p. 36, 2019. [Online]. Available: https://goo.gl/t2GgTW
[57] ABB, "IEC 60034-30-1 standard on efficiency classes for low voltage AC motors," 2019. [Online]. Available: https://goo.gl/qvLUzr
[58] Ricardo, "Ricardo develops next-generation electric vehicle motor," 2015. [Online]. Available: https://goo.gl/CGH8tH
[59] R. John, "MotorBrain summary report: Nanoelectronics for Electric Vehicle Intelligent Failsafe PowerTrain," Tech. Rep., 2015. [Online]. Available: http://www.motorbrain.eu/
[60] M. Kimiabeigi, J. D. Widmer, R. Long, Y. Gao, J. Goss, R. Martin, T. Lisle, J. M. Soler Vizan, A. Michaelides, and B. Mecrow, "High-performance low-cost electric motor for electric vehicles using ferrite magnets," *IEEE Transactions on Industrial Electronics*, vol. 63, no. 1, pp. 113–122, 2016.
[61] J. Merwerth, J. Halbedel, and G. Schlangen, "Electrical drive motor for a vehicle," 2012. [Online]. Available: https://goo.gl/WiLsMq
[62] I. Boldea, L. Tutelea, L. Parsa, and D. Dorrell, "Automotive electric propulsion systems with reduced or no permanent magnets: An overview," *IEEE Transactions on Industrial Electronics*, vol. 61, no. 10, pp. 5696–5711, 2014.
[63] S. M. De Pancorbo, G. Ugalde, J. Poza, and A. Egea, "Comparative study between induction motor and Synchronous Reluctance Motor for electrical railway traction applications," *2015 5th International Conference on Electric Drives Production, EDPC 2015 - Proceedings*, pp. 2–6, 2015.
[64] J. J. Germishuizen, F. S. Van Der Merwe, K. Van Der Westhuizen, and M. J. Kamper, "Performance comparison of reluctance synchronous and induction traction drives for electrical multiple units," *IEEE Transactions on Industry Applications*, pp. 316–323, 2000.
[65] N. Bianchi, S. Bolognani, E. Carraro, M. Castiello, and E. Fornasiero, "Electric Vehicle Traction Based on Synchronous Reluctance Motors," *IEEE Transactions on Industry Applications*, vol. 52, no. 6, pp. 4762–4769, 2016.
[66] VOLVO, "Power take-offs: Fields of application and Calculation guide," 2018. [Online]. Available: http://productinfo.vtc.volvo.se/files/pdf/lo/PowerTake-off(PTO)_Eng_08_580114.pdf
[67] ——, "Volvo Trucks - Premiere for our first all-electric truck," 2018. [Online]. Available: https://www.youtube.com/watch?v=zAbbulKiX-o
[68] ——, "Premiere for Volvo Trucks first all-electric truck," 2018. [Online]. Available: https://www.volvogroup.com/content/dam/volvo/volvo-group/markets/global/en-en/news/2018/apr/180412-volvo-all-electric-truck--en-2018-04-12-08-30-54.pdf
[69] ——, "Body builder instructions: PTO and pumps," 2018. [Online]. Available: https://www.volvotrucks.ca/en-ca/parts-and-services/service/body-builder/manuals/
[70] W. L. Soong, "Design and Modelling of Axially-Laminated Interior Permanent Magnet Motor Drives for Field-Weakening Applications," Ph.D. dissertation, Universitiy of Glasgow, 1993.
[71] A. K. Adnanes, "Torque Analysis of Permanent Magnet Synchronous Motors," *IEEE Transactions on Industry Applications*, pp. 695–701, 1991.
[72] J. Goss, "The Design of AC Brushless Permanent Magnet Motors for Electric Vehicle Traction Applications," Ph.D. dissertation, University of Bristol, 2015.

Branko Ban was born in Šibenik (Croatia) in 1991. He completed Bachelor (2012.) and Master (2015.) studies in Electrical Engineering at the University of Zagreb (Faculty of electrical engineering and computing) and Chalmers University of Technology. Since 2015. he is a part of the ALTEN consultancy team working in the automotive sector as electric machine specialist in areas related to design, advanced engineering, quality assurance, and root cause analysis. He is currently enrolled in the University of Zagreb PhD program covering next-generation electric machines.

Stjepan Stipetić was born in Ogulin (Croatia) in 1985. He received Dipl.Eng. and PhD degrees in electrical engineering from the University of Zagreb, Croatia, in 2008 and 2014, respectively. Currently, he is an Assistant Professor at the University of Zagreb Faculty of Electrical Engineering and Computing, Department of Electrical Machines Drives and Automation, Croatia where his research activities are related to design, modelling, analysis and optimization of electrical machines.

Mario Klanac was born in Zadar, Croatia. He received M.Sc. degree in electrical engineering from the University of Zagreb, Croatia in 2018. Currently, he is a research assistant at the University of Zagreb, Faculty of Electrical Engineering and Computing, Department of Electrical Machines, Drives and Automation, Croatia. His research interests include design, modeling, analysis and optimization of electrical machines.